Fracture and Toughening Behavior of Aramid Fiber/Epoxy Composites

Lei Wang, Wuiwui Chauhari Tjiu, Su Fern Teh, Chaobin He
Institute of Materials Research and Engineering, 3 Research Link, Singapore 117602

Tianxi Liu
Institute of Advanced Materials, Fudan University, 220 Handan Road, Shanghai 200433, P.R. China

The effect of short Aramid fibers on the fracture and toughening behavior of epoxy with high glass transition temperature has been studied. Fine dispersion of the fibers throughout the matrix is evidenced by optical microscopy. Compared with neat epoxy resin, the fracture toughness (K_{IC}) of the composites steadily increases with increasing fiber loading, indicating that addition of Aramid fibers has an effective toughening effect to the intrinsically brittle epoxy matrix. Scanning electron microscopy (SEM) indicates that formation of numerous step structures for fiber-filled epoxy systems is responsible for the significant toughness improvement. SEM and transmitted optical microscopy show that fiber pullout and fiber breakage are the main toughening mechanisms for the Aramid fiber/epoxy composites. POLYM. COMPOS., 26:333–342, 2005. © 2005 Society of Plastics Engineers

INTRODUCTION

Thermosets are highly cross-linked polymers with a three-dimensional molecular structure. The network structure gives rise to high stiffness, high strength, and good heat and solvent resistance, which make thermosets to be frequently used as structure materials. However, the network structure also results in a major drawback of thermosets: poor resistance to impact and crack initiation. Therefore, many efforts have been made to improve the fracture toughness of thermosets while still maintaining their other desirable properties. Epoxy resins are among the strongest thermosets and are the most extensively used class of thermosets in structural applications. Consequently, most investigations on the toughening of thermosets have mainly focused on epoxy systems [1–10]. One approach to toughening epoxies is addition of second phase polymeric particles, such as rubber and thermoplastics [9–11]. Rubber toughening is the most thoroughly studied route to improve the properties of epoxies. However, the toughening effect is achieved only for large rubber particles that possess good adhesion with the epoxy matrix, and usually it is not effective in toughening epoxies with high cross-linking densities.

Fiber-reinforced epoxies are of great potential for use in the primary structures of aircraft and automobiles. They are generally manufactured by using fibers as reinforcement and epoxy resin as a matrix. One of the most popular fibers is carbon fibers. Carbon fiber–reinforced epoxies show several desirable properties such as high modulus, high strength, and good stiffness. However, these composites are very susceptible to impact damage. One of the approaches to improve the mechanical properties is to use ductile fibers such as polyethylene (PE) [12], polypropylene [13], and Aramid (Kevlar) fibers [14] as reinforcement.

The pioneering work by Wang et al. [15], Li et al. [16], and Li and Mohamed [17] on toughening of brittle inorganic cement matrix by using ultradrawn PE fibers is intriguing. With an addition of only 1 vol% of PE fibers, the fracture toughness of cement matrix can be improved by an order of magnitude. Multitudes of toughening mechanisms, e.g., crack blunting, crack bridging, microcracking, fiber pullout, and fiber-matrix debonding induced strain-hardening, have been observed and found to be responsible for such an impressive fracture toughness improvement. Cement material is known to be extremely brittle and incapable of undergoing any plastic deformation. The presence of only 1 vol% of PE fibers to induce so many toughening mechanisms in cement is truly impressive.

In this article, we use a similar approach described by Li et al. [16,17] to toughen intrinsically brittle and high cross-linking density epoxy. In order to achieve maximum reinforcement, strong fibers with good compatibility with the matrix are required. Aramid fibers are good candidates as reinforcement due to their excellent properties. The main goals of this study are to fabricate Aramid fiber filled epoxy

Correspondence to: T. Liu; e-mail: txliu@fudan.edu.cn or C. He; e-mail: cb-he@imre.a-star.edu.sg
DOI 10.1002/pc.20101
Published online in Wiley InterScience (www.interscience.wiley.com).
© 2005 Society of Plastics Engineers

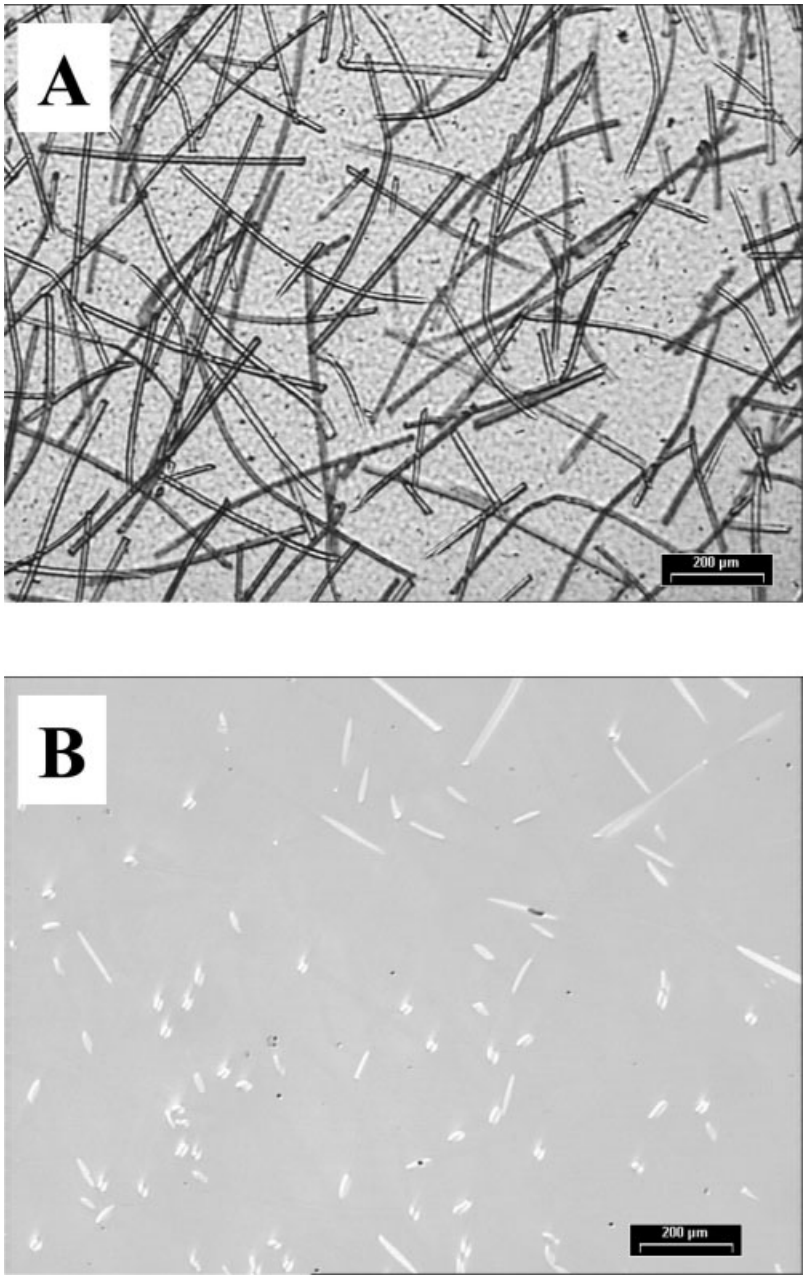

FIG. 1. Optical microscopy observations on fiber dispersion for epoxy composite containing 3 wt% Aramid fibers. A: Transmitted mode. B: Reflected mode.

composites with high fracture toughness and to study their fracture behavior and toughening mechanism(s).

EXPERIMENTAL

Materials

An aromatic epoxy, diglycidyl ether of bisphenol A (DGEBA) in the form of DER332 from Dow Chemical, was chosen for the study. This epoxy resin possesses epoxide equivalent weight of 171–175, viscosity of 4–6 Pa · s, and specific gravity of 1.16 at 25°C. The curing agent, Ethacure 100LC from Albemarle Co. is aromatic diethyltoluene diamine (DETDA), which is widely used in high performance epoxy resins. Ethacure 100LC is a mixture of two DETDA isomers, containing 75–81% 2,4 isomer and 18–20% 2,6 isomer. Aramid short fibers (Connex) with length of about 0.6 mm and average diameter of about 15 μm were kindly provided by Teijin Co.

Sample Preparation

Chemicals were dried in vacuum oven for 12 hrs at 80°C prior to sample preparation. The composites were prepared by mechanically mixing the short fibers and liquid epoxy resin together using a high-speed homogenizer at 10,000 rpm. When a homogeneous dispersion of fibers was achieved, a stoichiometric amount of curing agent was

added. The blends were mechanically stirred and degassed for 2 hrs to eliminate bubbles. The degassed mixture was poured into a preheated and vertically mounted glass mold in an oven and was cured for 2 hrs at 100°C followed by postcuring for 5 hrs at 180°C. After that, the oven was switched off and the cured resin was allowed to cool slowly to room temperature in the oven. The results from the first and second runs by using differential scanning calorimetry (not shown here for abbreviation) indicate that the samples are fully cured. The glass transition temperature of the cured epoxy resin was determined to be 210°C by dynamic mechanical analysis. The obtained plates (with thickness of about 6.25 mm) were finally machined into rectangular bars for subsequent mechanical (bending) tests.

Mechanical Testing and Characterizations

The mode I fracture toughness, as quantified by the critical stress intensity factor (K_{IC}), was determined using the three-point bending (3PB) test. Single-edge-notched (SEN) specimens were machined with thickness (B) and width (W) of 6.25 and 12.5 mm, respectively. This specimen geometry satisfies the requirements for the plane strain conditions (ASTM E399). A sharp notch was introduced by tapping a hammer on a fresh single-edge razor blade inserted into the sample. The tip of the crack was created by the wedging action of the blade. The 3PB experiments were performed at room temperature using a computer-controlled Instron machine (Mode 5567) at a crosshead speed of 2 mm/min and with a span of 50 mm. The K_{IC} values were determined using the following relationship [18, 19]:

$$K_{IC} = Y\frac{3PS\sqrt{a}}{2BW^2} \quad (1)$$

$$Y = 1.93 - 3.07(a/W) + 14.53(a/W)^2 - 25.11(a/W)^3 + 25.80(a/W)^4 \quad (2)$$

where Y is a shape factor, P the load at failure, S the length of the span, and a the crack length. At least six specimens for each composition were tested.

The morphologies of the fracture surfaces of the tested SEN-3PB specimens were observed using scanning electron microscopy (SEM) (JEOL-JSM-5600) under an accelerating voltage of 5 kV. Prior to SEM observation, the fracture surfaces were coated with a thin layer of gold.

The double-edge-notched four-point bending (DEN-4PB) technique [20] was used to create subcritically loaded cracks. First, specimens (with dimension of 6.25 × 12.5 × 90 mm^3) having two almost identical cracks on the same edge were prepared and fractured in 4PB geometry [20]. Since the two cracks cannot be identical, upon bending test (at a speed of 2 mm/min) one of the cracks will grow subcritically and stop before failure, while the other breaks. After the subcritically-loaded cracks were prepared, the DEN-4PB samples were polished to about 80 μm in thickness. The morphologies of the thin sections were examined using an optical microscope under transmitted (bright field and crossed polars) mode.

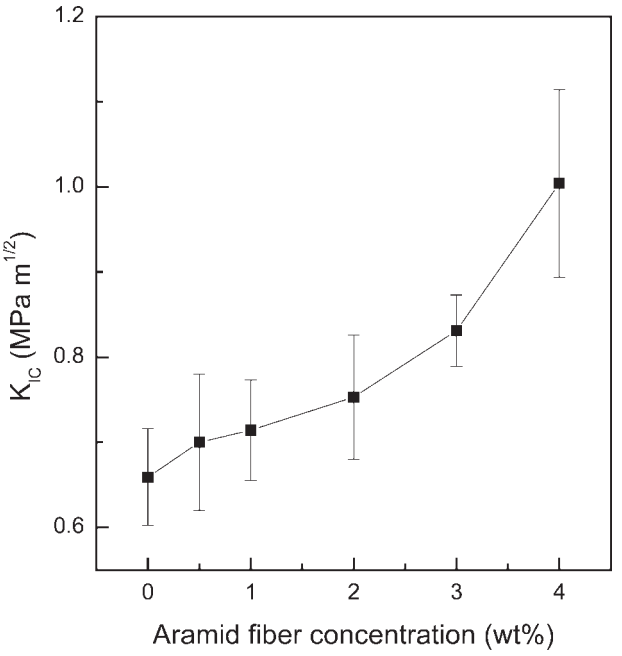

FIG. 2. Dependence of fracture toughness on fiber concentration for Aramid fiber/epoxy composites.

RESULTS AND DISCUSSION

Fiber Dispersion

A fine dispersion of the fibers throughout the matrix is necessary to achieve good properties for the composites. For instance, a cluster of short fibers, instead of uniform dispersed fibers, will weaken the composites due to the fact that the fibers inside the clusters are probably not contributing to the property improvement. These clusters may even act as actual failure sites. Optical micrographs shown in Fig. 1 illustrate the fiber dispersion for the composite containing 3 wt% Aramid fibers, as an example. Transmitted optical microscopy (TOM) (Fig. 1A) shows that the chopped fibers are uniformly distributed and randomly oriented in the composite, with a length of about 0.6 mm and a diameter of about 10 μm. It can be also seen that most fibers are bent or curved and no fiber surface damage is observed, probably indicating that the fibers are ductile and strong. From ROM image (Fig. 1B), the elliptical shapes of cross-sections for some fibers (after polishing) are clearly identified, also indicating a random fiber orientation and homogeneous fiber dispersion within the epoxy matrix.

Fracture Toughness

The mode I fracture toughness, K_{IC}, as a function of the fiber concentration (wt%) of the composites is shown in Fig.

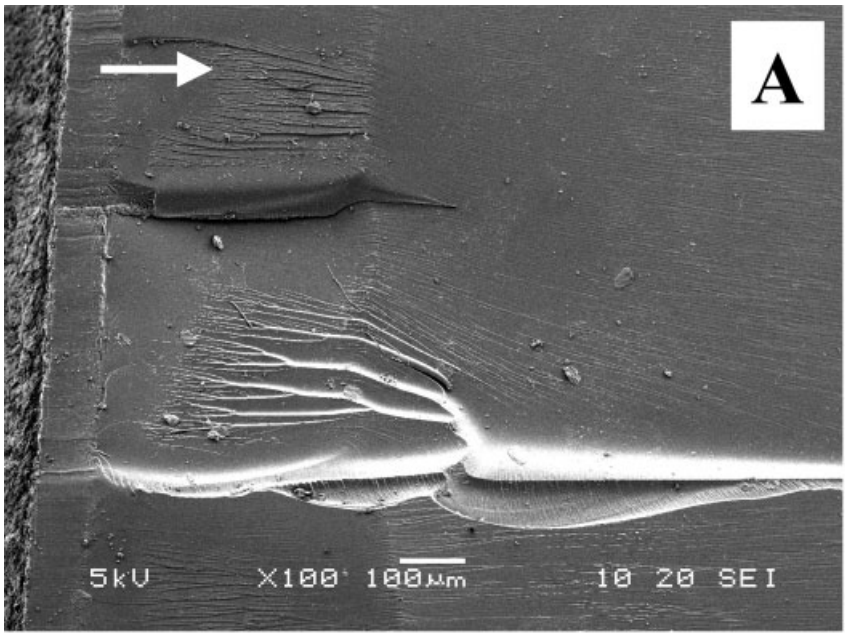

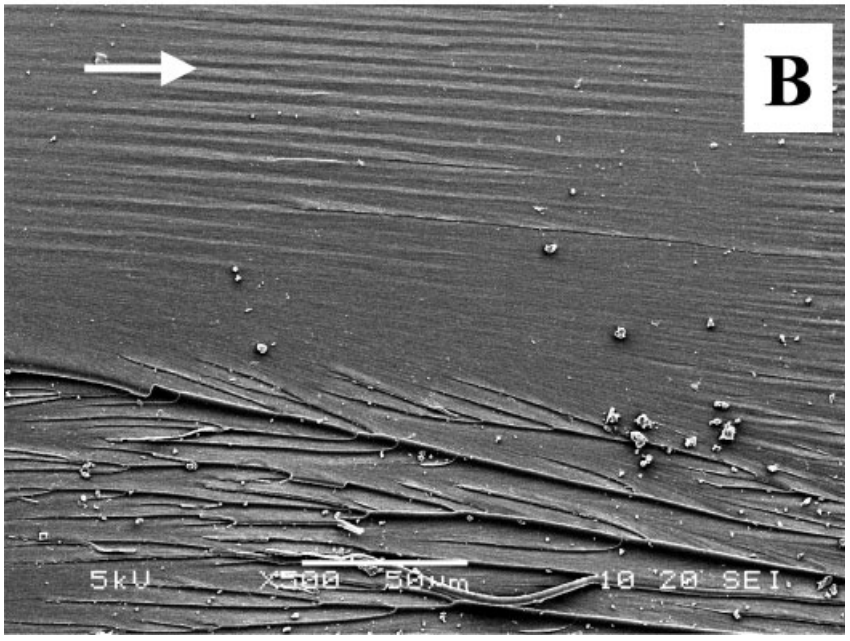

FIG. 3. SEM micrographs of the fracture surfaces of neat epoxy. A: ×100. B: ×500. Arrow indicates the crack propagation direction.

2. It can be seen that the fracture toughness steadily increases by about 54% with increasing fiber concentration, i.e., from 0.65 MPa · $m^{1/2}$ for neat epoxy resin to 1 MPa · $m^{1/2}$ for the composite containing 4 wt% Aramid fibers. In rubber [3,9] and clay [21] toughened epoxy systems, it has been reported that there exists an upper limit of the modifier content beyond which the toughness of the composite does not increase and even declines. In Fig. 2, the K_{IC} values of Aramid fiber filled epoxy systems increase even faster with increasing fiber concentration. Therefore, further improvement on the fracture toughness may be expected upon addition of more Aramid fibers into epoxy matrix. However, achieving homogeneous fiber dispersion will probably become difficult when incorporating more fibers into the matrix.

Toughening Mechanisms

Toughening mechanisms such as crack bowing, crack deflection, interface debonding, fiber pullout, and wake toughening may be operative in a composite [22]. In a given composite more than one toughening mechanisms are likely to be operating, although one mechanism may dominate. Effectiveness of the toughening mechanism mainly depends to some extent on: 1) size, morphology and volume fraction of the reinforcement; 2) interfacial bonding strength; 3)

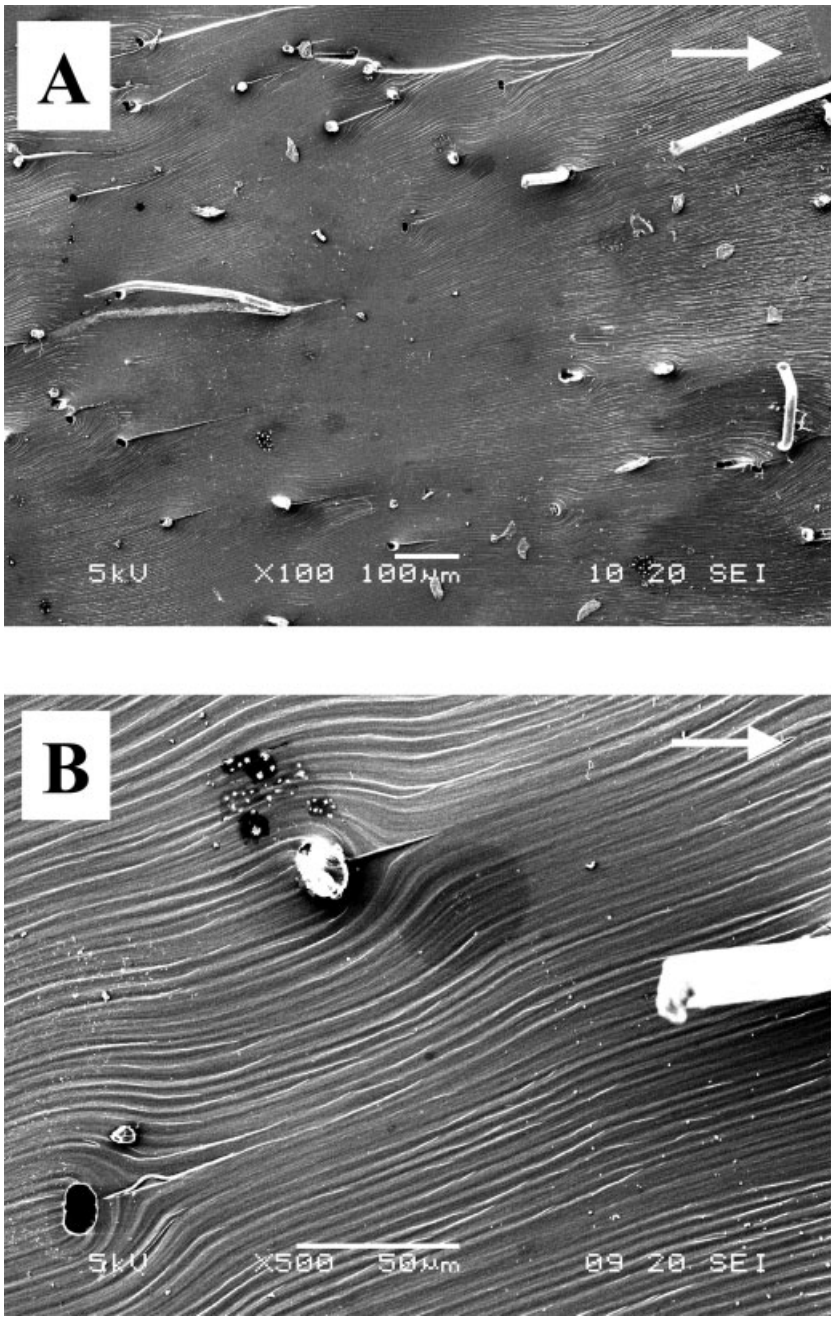

FIG. 4. SEM micrographs of the fracture surfaces of epoxy composite containing 1 wt% Aramid fibers. A: ×100. B: ×500. Arrow indicates the crack propagation direction.

properties (e.g., mechanical property, thermal expansion) of the matrix and the reinforcement; and 4) phase transformations.

To understand the fracture behavior and the toughening mechanisms in the systems studied here, the fracture surfaces (only within process zone [23]) of Aramid fiber–filled epoxy were examined using SEM. Figure 3 shows the fracture surfaces of neat epoxy at low (Fig. 3A) and high (Fig. 3B) magnifications. It can be seen that for neat epoxy resin the fracture surface is quite smooth, indicating a typical brittle failure nature. Compared with the case in neat epoxy, Fig. 4 illustrates much rougher fracture surfaces of the composite containing 1 wt% Aramid fibers at low (Fig. 4A) and high (Fig. 4B) magnifications. It clearly shows some holes originated from the pullout of the fibers, indicating that the interfacial adhesion between the fibers and the matrix is not that strong. In addition, at higher magnification (Fig. 4B), numerous river structures are observed on the fracture surface of the composite. Some steps parallel to the direction of crack propagation can be also seen behind the fibers and the holes, which are the characteristic tail structures formed when two secondary crack fronts (separated by a fiber or a hole) meet with each other [24–26]. Usually, the crack propagation planes of secondary cracks cannot be perfectly coplanar. The interaction between the reinforcement and the crack front causes the crack to be

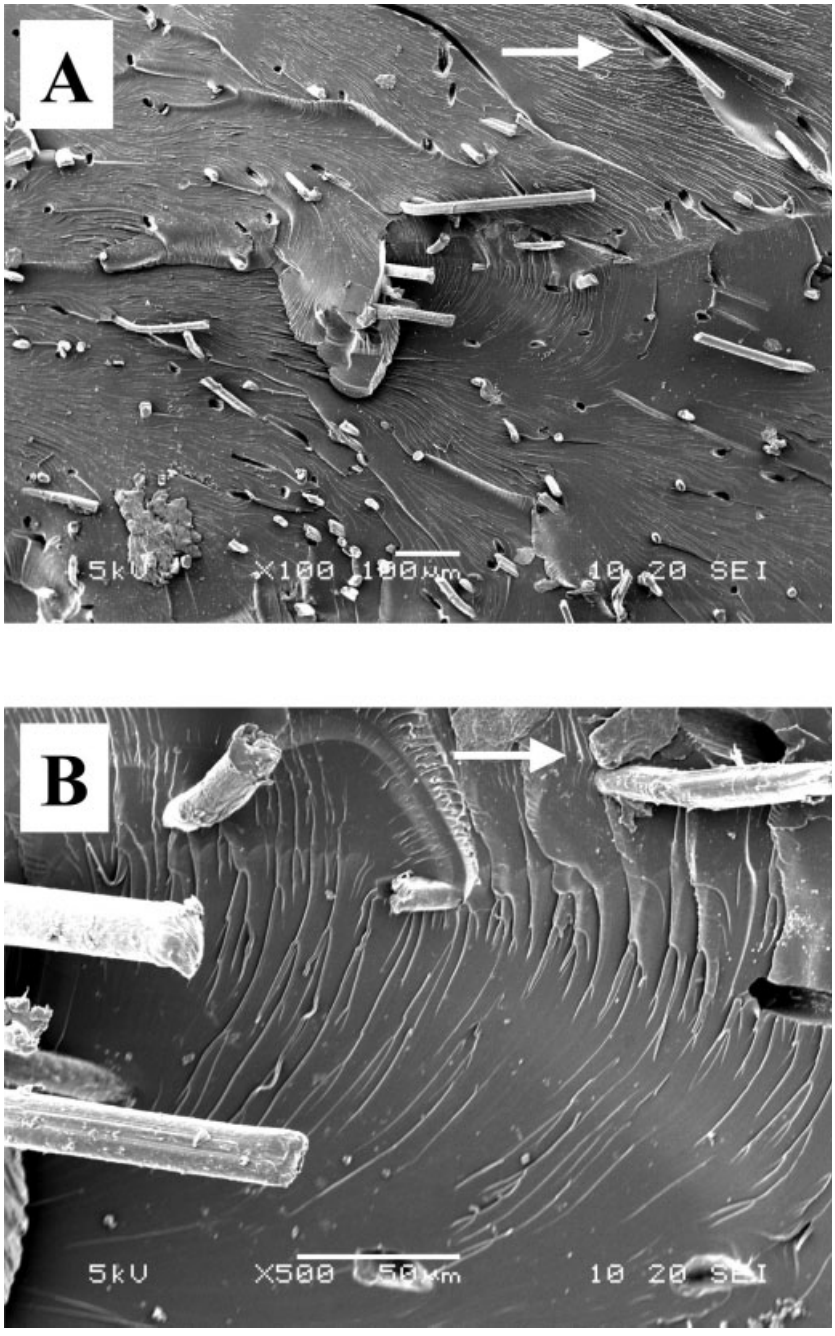

FIG. 5. SEM micrographs of the fracture surfaces of the composite containing 4 wt% Aramid fibers. A: ×100. B: ×500. Arrow indicates the crack propagation direction.

deflected and to become non-planar. In this case, crack propagation is hindered, as often observed in glass bead–filled epoxy composites [27, 28]. Appearance of these structures indicates that the crack front goes around the fibers when it meets with them and then proceeds further. As the crack opens under the action of applied stress, some of the stress is transferred to the fibers, which then deform elastically. During this process, some fibers break and the others were debonded and pulled out. Wake toughening and fiber bridging, in this case, may also occur. All these operative mechanisms may contribute to the fracture toughness improvement in the composites, as shown in Fig. 2.

At higher fiber loading, for example 4 wt% as shown in Fig. 5 in different magnifications, the fracture surfaces of the composite become much more rougher. In addition to the above phenomena observed in the case of 2 wt% fiber–filled epoxy system (see Fig. 4), one can also see the following: 1) Besides intimate contact between the fibers and the matrix, many fibers break, indicating that the interfacial adhesion between the fibers and the matrix is not that poor. 2) After failure, the fiber surfaces are quite rough, with residual epoxy fragments around the fibers, probably suggesting a cohesive failure in the matrix. 3) Most pulled out fibers have similar orientation, which is parallel to the crack propagation direction, while the broken fibers show different inclining angles relative to the crack propagation direction. The maximum load required to pull out the fibers varies with different inclining angles [16] to make these

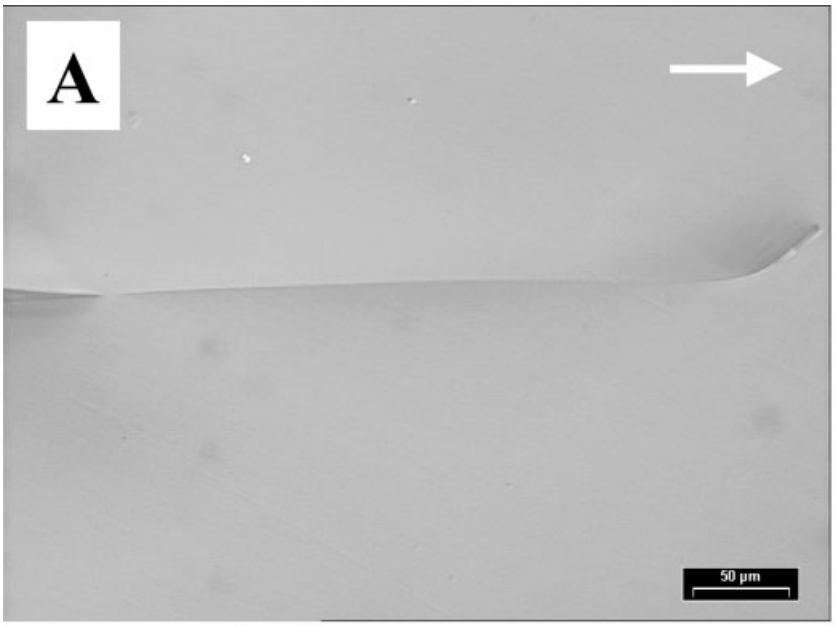

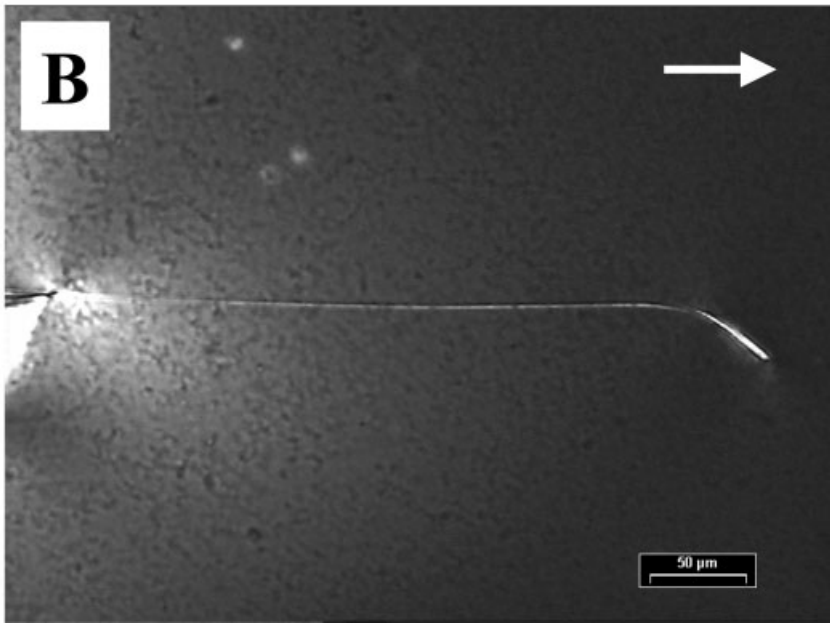

FIG. 6. Transmitted optical micrographs of crack tip damage zone for neat epoxy. A: TOM image. B: Birefringence image under cross polars. Arrow indicates the crack propagation direction.

fibers relatively easy to be pulled out. 4) In the central region of Fig. 5A, a big "cave" structure can be seen, which is often observed in the composites with high fiber loading. In this case, several fibers may be closely arrayed and parallel to each other to form a fiber group. When the crack fronts meet this fiber group and try to pull them out, the neighboring epoxy matrix around them experiences a very high stress. As a result, a patch of epoxy matrix was torn off instead of the fibers. Consequently, the step structures (formed after the torn-off matrix) are quite different from the river morphology. Instead, along the crack propagation direction many ripple morphologies are always observed on the fracture surfaces for the composites with high fiber contents, as shown at high magnification in Fig. 5B. Therefore, a large amount of energy is absorbed and dissipated through shearing and tearing of epoxy matrix during this failure process. These caves are often observed in the composites with high fiber concentrations. Recalling the results in Fig. 2, in which the K_{IC} values increase even faster at higher fiber concentrations, the formation of these cave structure or ripple morphology is probably responsible for the significant toughness improvement.

Figure 6A and B show optical micrographs of the process zone in front of a surviving "subcritical" crack in the neat epoxy, taken under bright-field and cross-polarized light, respectively. It can be seen that for neat epoxy, the

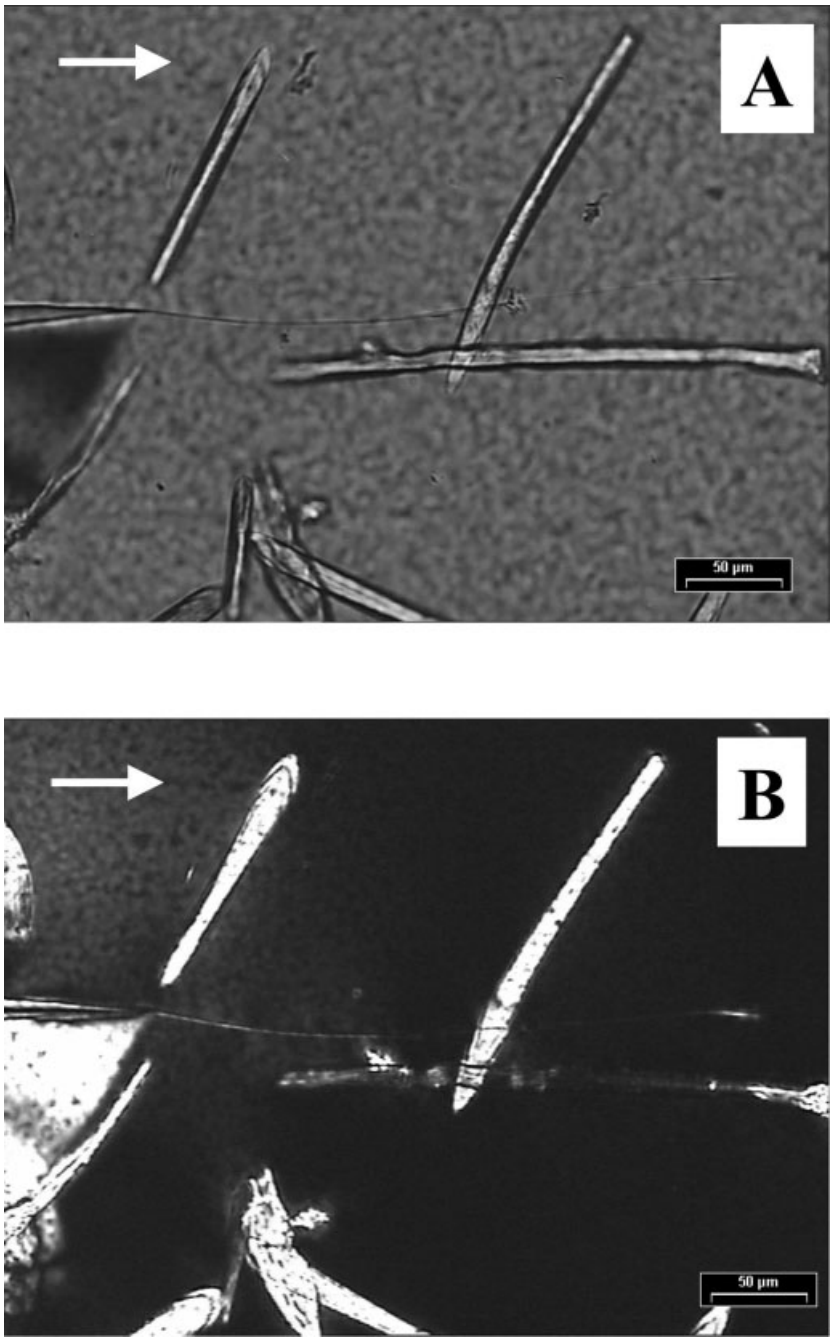

FIG. 7. Transmitted optical micrographs of crack tip damage zone for the composite containing 2 wt% Aramid fibers. A: TOM image. B: Birefringence image under cross polars. Arrow indicates the crack propagation direction.

crack propagates in a straight and sharp manner, and almost no deformation zone or birefringence is observed in front of the crack tip, indicating that the material is intrinsically brittle without noticeable plastic deformation occurring upon fracture. For the composite containing 3 wt% Aramid fibers (Fig. 7A and B; for bright-field and birefringence, respectively), however, it can be seen that the crack front passes through a fiber at the crack tip damage region and stops at a neighboring fiber before it can break or pull out the former fiber. Under birefringence mode (under cross-polarized light), it can be seen that plastic deformation occurs in the interfacial region between the fibers and the matrix. This may be caused by the shear strength of interfacial debonding between the fibers and the matrix. Figure 8A and B illustrate another toughening mechanism observed in the composite with 4 wt% fibers—fiber breakage, which is also supported by SEM observations in Fig. 5. It can be seen that the fibers were directly pulled out by the proceeding crack front with no interfacial debonding as evidenced by TOM, indicating that Aramid fibers have (modest) good interfacial adhesion with the epoxy matrix. Additionally, an attempt is being made to modify the surfaces of Aramid fibers to further enhance the interfacial adhesion between the fibers and the epoxy matrix. The effect of fiber surface treatment on fracture behavior of the composites will be reported separately.

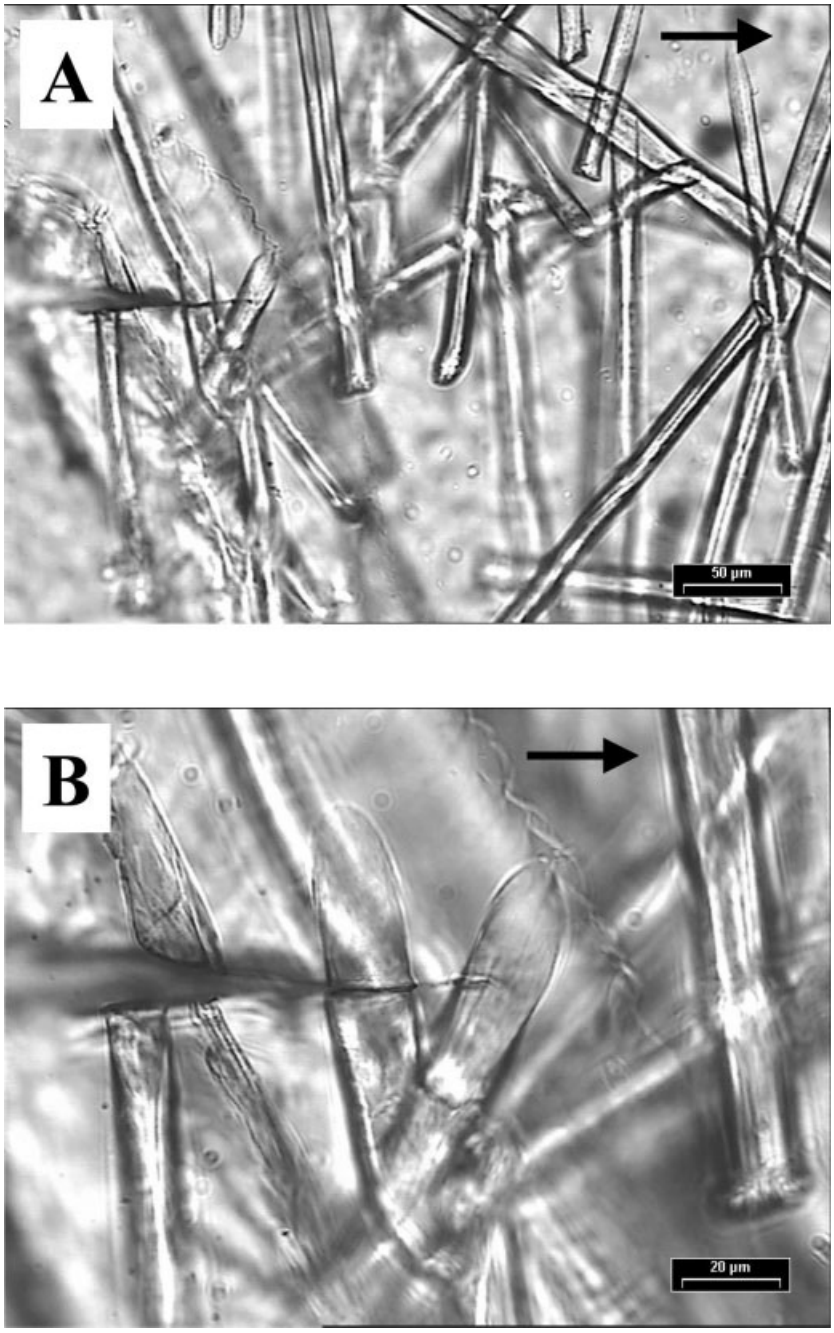

FIG. 8. Transmitted optical micrographs (at different magnifications) of crack tip damage zone for the composite containing 4 wt% Aramid fibers. Arrow indicates the crack propagation direction.

CONCLUSIONS

Short Aramid fiber–filled epoxy composites have been prepared as a function of fiber loading. The fibers are homogeneously dispersed and randomly oriented throughout the matrix by morphological observation. The fracture toughness (K_{IC}) steadily increases with increasing fiber concentration, e.g., improving by about 54% from 0.65 MPa · $m^{1/2}$ for neat epoxy resin to 1.0 MPa · $m^{1/2}$ for the composite containing only 4% Aramid fibers. SEM and TOM observations on the fracture surfaces and the crack tip damage zones of the composites indicate that formation of step structures, fiber pullout, and fiber breakage are probably the dominant mechanisms accounting for the K_{IC} increase. In addition, matrix shearing and tearing also contribute much to the fracture toughness improvement, especially at higher fiber loading. Therefore, considering the role of neighboring fibers on stress transfer between the resin and the fibers, the effects between local and global load sharing might be of importance here, especially while the improvements in K_{IC} at low fiber loading levels is modest, and the improvement becomes significant once a threshold volume fraction is attained. It clearly seems that above this threshold concentration the advancing crack is frequently met with a fiber in its path propagation whereas at low fiber concentration, the crack traverses through patches of pure resin in which it meets little resistance to propagate.

NOMENCLATURE

PE:	polyethylene
DGEBA:	diglycidyl ether of bisphenol A
DETA:	diethyltoluene diamine
K_{IC}:	critical stress intensity factor
SEN-3PB:	single-edge-notch three-point bending test
DEN-4PB:	double-edge-notched four-point bending test
SEM:	scanning electron microscopy
TOM:	transmitted optical microscopy
ROM:	reflected optical microscopy

REFERENCES

1. A.C. Meeks, *Polymer*, **15**, 675 (1974).
2. S.C. Kunz and P.W.R. Beaumont, *J. Mater. Sci.*, **16**, 3141 (1981).
3. A.F. Yee and R.A. Pearson, *J. Mater. Sci.*, **21**, 2462 (1986).
4. R.A. Pearson and A.F. Yee, *J. Mater. Sci.*, **24**, 2571 (1989).
5. A.F. Yee, D. Li, and X. Li, *J. Mater. Sci.*, **28**, 6392 (1993).
6. Y. Huang and A.J. Kinloch, *J. Mater. Sci.*, **27**, 2753 (1992).
7. Y. Huang and A.J. Kinloch, *J. Mater. Sci.*, **27**, 2763 (1992).
8. H.J. Sue, *Polym. Eng. Sci.*, **31**, 275 (1991).
9. R. Bagheri and R.A. Pearson, *Polymer*, **37**, 4529 (1996).
10. R. Bagheri and R.A. Pearson, *Polymer*, **41**, 269 (2000).
11. J. Du, M.D. Thouless, and A.F. Yee, *Int. J. Fract.*, **92**, 271 (1998).
12. T. Ogawa, H. Mukai, and S. Osawa, *J. Appl. Polym. Sci.*, **79**, 1162 (2001).
13. R.C.L. Dutra, B.G. Soares, E.A.Campos, J.D.G. De Melo, and J.J.G. Silva, *J. Appl. Polym. Sci.*, **73**, 69 (1999).
14. R.J. Young, M.C. Andrews, and N. Rallis, *Composites A.*, **27**, 889 (1996).
15. Y.J. Wang, S. Backer, and V.C. Li, *J. Mater. Sci.*, **22**, 4281 (1987).
16. V.C. Li, Y.J. Wang, and S. Backer, *Composites A.*, **21**, 132 (1990).
17. V.C. Li and M. Mohamed, *Cement Concrete Composites*, **18**, 239 (1996).
18. W.F. Brown and J.E. Srawley, *ASTM STP*, **381**, 13 (1965).
19. R.W. Hertzberg, *Deformation and Fracture Mechanics of Engineering Materials*, Wiley, New York (1989).
20. H.J. Sue and A.F. Yee, *J. Mater. Sci.*, **28**, 2975 (1993).
21. A.S. Zerda and A.J. Lesser, *J. Polym. Sci. Polym. Phys.*, **39**, 1137 (2001).
22. D.L. Mattews and R.D. Rawlings, *Composite Materials: Engineering and Science*, CRC Press, Boca Raton, FL (1999).
23. R.A. Pearson and A.F. Yee, *J. Mater. Sci.*, **21**, 2475 (1986).
24. F.F. Lange, *Philos. Mag.*, **22**, 983 (1970).
25. J. Spanoudakis and R.J. Young, *J. Mater. Sci.*, **19**, 473 (1984).
26. J. Spanoudakis and R.J. Young, *J. Mater. Sci.*, **19**, 487 (1984).
27. J. Lee and A.F. Yee, *Polymer*, **41**, 8375 (2000).
28. J. Lee and A.F. Yee, *Polymer*, **42**, 577 (2001).